

## Supporting Information

# Control Over Products Formation and Thermodynamic Stability of Thiolate-Protected Gold Nanoclusters Through Tuning of Surface Protecting Ligands

*Manju P. Maman,<sup>[a]</sup> Eyyakkandy Nida Nahan,<sup>[a]</sup> Greeshma Suresh,<sup>[a]</sup> Arunendu Das,<sup>[b]</sup> Akhil S. Nair,<sup>[b]</sup> Biswarup Pathak,<sup>[b]</sup> Sukhendu Mandal<sup>[a]</sup> \**

<sup>a</sup> School of Chemistry, Indian Institute of Science Education and Research Thiruvananthapuram, Kerala 695551, India. Email: [sukhendu@iisertvm.ac.in](mailto:sukhendu@iisertvm.ac.in)

<sup>b</sup> Department of Chemistry, Indian Institute of Technology, Indore, Madhya Pradesh 453552, India.

## Table of contents

Name	Description	Page No.
	General Information	S3-7
	References	S8
Figure S1	UV-visible spectrum and ESI-MS of Au <sub>10</sub> (TBBT) <sub>10</sub>	S9
Figure S2	Time dependent MALDI-MS of ligand exchange with BT ligand	S10
Figure S3	Characterization of SEC bands obtained in case of 4-TBBT	S11
Figure S4	Characterization of SEC bands obtained in case of 4-IBT	S12
Figure S5	Characterization of SEC bands obtained in case of 4-EBT	S13
Figure S6	Characterization of SEC bands obtained in case of 4-MBT	S14
Figure S7	Characterization of SEC bands obtained in case of BT	S15
Figure S8	UV-visible spectra showing the stability test of Au <sub>36</sub> (SR) <sub>24</sub>	S16
Figure S9	Different kernel structures with their respective type of staple motif	S17
Figure S10	Optimized structure of [Au <sub>23</sub> (SR) <sub>16</sub> ] <sup>-</sup> , [Au <sub>25</sub> (SR) <sub>18</sub> ] <sup>-</sup> and [Au <sub>28</sub> (SR) <sub>20</sub> ]	S18
Figure S11	Rotational barrier for [Au <sub>23</sub> (TBBT) <sub>16</sub> ] <sup>-</sup> , [Au <sub>25</sub> (TBBT) <sub>18</sub> ] <sup>-</sup> , and Au <sub>28</sub> (TBBT) <sub>20</sub> clusters	S19
Table S1	Calculated values of average ligand removal reaction energy (LRE) and rotational barrier for Au <sub>n</sub> (TBBT) <sub>m</sub> clusters	S20
Table S2	Formation energy (FE) values for all thiol ligands in [Au <sub>25</sub> (SR) <sub>18</sub> ] <sup>-</sup> clusters	S20
Figure S12	Optimized structure of [Au <sub>25</sub> (IBT) <sub>18</sub> ] <sup>-</sup> and [Au <sub>25</sub> (TBBT) <sub>18</sub> ] <sup>-</sup> clusters	S21
Table S3	Rotational barrier values for thiol based IBT and TBBT ligand in [Au <sub>25</sub> (SR) <sub>18</sub> ] <sup>-</sup> clusters	S22
Table S4	Core cohesive energy (CE) and shell to core binding energy (CSBE) of all Au <sub>n</sub> (SR) <sub>m</sub> clusters	S22
Table S5	Reaction energy (RE) values (eV) for all the conversion process	S23
Table S6	Average ligand interaction energy (eV/SR) of all the Au <sub>n</sub> (SR) <sub>m</sub> clusters	S23
Table S7	Core cohesive energy (CE), shell to core binding energy (CSBE), average ligand interaction energy (LI) values of intermediate [Au <sub>25</sub> (SR) <sub>18</sub> ] <sup>-</sup> clusters and reaction energy (RE) values for Reaction-IIIz	S24
Figure S13	Reaction energy (RE) following Reaction-III	S25
Figure S14	Alternative view of a proposed cluster of Au <sub>26</sub> core along with dissociating cyclic chair conformation of Au <sub>6</sub> unit composed of two Au <sub>3</sub> units	S26
Figure S15	Proposed mechanistic transformation of dissociating Au <sub>6</sub> unit with four dimeric staples	S27
Figure S16	Proposed mechanism for dissociation of Au <sub>6</sub> unit and symmetry assisted complex rearrangement of Au <sub>20</sub> core isomerization	S28

## General Information

### 1) Materials

Tetrachloroauric (III) acid trihydrate ( $\text{HAuCl}_4 \cdot 3\text{H}_2\text{O}$ , > 99.99 % metals basis), Cyclohexanethiol (CHT, 98 %), sodium borohydride ( $\text{NaBH}_4$ , 99.99 %, trace metal basis), tetraoctylammoniumbromide (TOAB, 98%), 4-tert-butylbenzenethiol (TBBT, 97 %), 4-methylbenzenethiol (4-MBT, 98 %), trans-2-[3-(4-tert-butylphenyl)-2-methyl-2 propenylidene] malononitrile (DCTB, > 99.0 %) were purchased from Sigma Aldrich. 4-ethylthiophenol (4-EBT, 97 %), and Thiophenol (TP/BT, 99 %) was purchased from Alfa-Aesar. 4-Isopropylbenzenethiol (4-IBT, 94 %) was purchased from Tokyo Chemical Industry (TCI) chemicals. Bio-Beads S-X1 beads- styrene divinylbenzene beads for SEC, 1 % cross-linkage, 40-80  $\mu\text{m}$  bead size, 600-14000 MW exclusion range was purchased from Bio-rad. Solvents used were methanol (HPLC grade, 99.9 %, Spectrochem), toluene (HPLC grade, 99.9 %, Spectrochem), Dimethylene chloride (DCM, HPLC grade, 99.9 %, Spectrochem).

### 2) Synthesis of $[\text{Au}_{23}(\text{CHT})_{16}]^-$ nanocluster

According to the reported procedure,<sup>S1</sup>  $\text{HAuCl}_4 \cdot 3\text{H}_2\text{O}$  (0.3 mmol, 118 mg) and tetraoctylammonium bromide (TOAB, 0.348 mmol, 190 mg) were dissolved in methanol (15 mL) in a 50 mL round-bottom flask. After vigorously stirring for 15 min, the solution color changed from yellow to dark reddish orange. Then, excess 1-cyclohexanethiol (1.6 mmol, 196  $\mu\text{L}$ ) was added to the mixture at room temperature. The reddish orange solution turned yellowish. After ~15 min,  $\text{NaBH}_4$  (3 mmol, 114 mg dissolved freshly in 6 mL of cold nanopure water) was rapidly added to the solution under vigorous stirring. The solution turned black immediately indicating formation of Au clusters. After overnight stirring (12 h), the reaction mixture was precipitated out by using methanol and washed several times using same solvent. The purity of the obtained cluster was confirmed by using mass spectrometry and UV-visible spectroscopy.

**3) Ligand Exchange with SR (where SR = 4-TBBT, 4-IBT, 4-EBT and BT respectively)**

[Au<sub>23</sub>(CHT)<sub>16</sub>]<sup>-</sup> nanocluster (5 mg) was dissolved in 1 mL DCM and 250 μL of SR was added, then the reaction mixture was stirred at 500 rpm for 48 h at 40 °C (10 mL round bottom flask). After that, the solution was cooled down to RT, excess methanol was added to the reaction mixture to precipitate out the cluster and centrifuged. The so obtained cluster was washed several times with methanol and extracted with toluene.

**4) Ligand Exchange with 4-MBT**

[Au<sub>23</sub>(CHT)<sub>16</sub>]<sup>-</sup> nanocluster (5 mg) was dissolved in 1 mL DCM and 250 mg of SR was added, then the reaction mixture was stirred at 500 rpm for 48 h at 40 °C (10 mL round bottom flask). After that, the solution was cooled down to RT, excess methanol was added to the reaction mixture to precipitate out the cluster and centrifuged. The so obtained cluster was washed several times with methanol and extracted with toluene.

**5) Size Exclusion Chromatography (SEC):**

The reaction mixture obtained after 48 h/11 days of reaction was washed several times with methanol. The crude product was dried, weighed, dissolved in 1 mL toluene and centrifuged. The solid residue was separated from the reaction mixture dissolved in toluene. This procedure was repeated three times. Later the solvent was evaporated from the reaction mixture and dried under vacuum for overnight and weighed.

The soluble product obtained was further separated by size exclusion chromatography using S-X1 bio beads. The beads were soaked overnight in toluene for the beads to swell prior to packing the column. After the beads are fully swollen, these are packed into a chromatographic column and washed with toluene. The reaction mixture was dissolved in toluene and elution was performed in toluene solvent at a flow rate of 1 drop/min. The sample was loaded on the top of the column and allowed to run slowly. The different fractions were collected separately, characterized, vacuum dried and quantified.

**6) Characterization techniques**

The absorption spectra were collected at room temperature on a UV-3800 SHIMADZU UV-Vis NIR spectrometer using a 3.5 mL cuvette and DCM as solvent. The mass spectrum of the cluster samples was collected using a Bruker Microflex MALDI-TOF

mass spectrometer. The matrix used was DCTB, and a stock solution of DCTB was prepared with a concentration of 20 mg in 1 mL DCM. The sample was prepared as 1 mg in 100  $\mu$ L DCM. From the stock solution, various amounts of matrix solution were taken and mixed with 1  $\mu$ L of analyte solution. The molecules were ionized with the Nd: YAG laser ( $\lambda = 266$  nm). The matrix concentration was varied for optimization to get a well resolved spectrum. ESI-MS data of the compound was obtained by using Waters-Xevo-G2-XS-QToF instrument in positive mode. Sample preparation for ESI-MS was done by dissolving 1 mg analyte in 1 mL of DCM and mixed with 1 mL of 50 mM cesium acetate in methanol in 1:1 v/v.

## 7) Computational Details: Text S1.

The density functional theory (DFT) calculations are carried out using the Projector augmented wave (PAW) method, as implemented in the Vienna Ab Initio Software Package (VASP).<sup>S2,S3</sup> The generalized gradient approximation of Perdew–Burke–Ernzerhof (GGA-PBE) functional has been used for describing ion electron interactions.<sup>S4</sup> Furthermore, a 450 eV plane-wave cutoff energy has been used to expand electronic wave function. The ionic relaxations have been carried out using a conjugate gradient algorithm. The convergence criteria are set as  $1 \times 10^{-4}$  eV for the electronic energy and 0.05 eV  $\text{\AA}^{-1}$  for the force minimization. A  $30 \times 30 \times 30 \text{\AA}^3$  cubic supercell was used to keep sufficient distance between two successive periodic images of nanoclusters. The Brillouin zone was sampled with a Gamma point ( $1 \times 1 \times 1$ ). All the calculations were performed without any spin restrictions.

The ligand removal reaction energy (LRE) is calculated by following the equation;



Where  $E[\text{Au}_{25}(\text{SR})_{18}]^-$  is the total energy of  $\text{Au}_{25}(\text{SR})_{18}$  cluster,  $E[1/2\text{H}_2]$  is half the energy of gas phase  $\text{H}_2$ ,  $E[\text{Au}_{25}\text{S}_{18}(\text{R})_{17}]^-$  is the energy of the cluster with one 4-isopropyl benzene/4-tertbutylbenzene ligand removed for  $\text{SR} = \text{IBT/TBBT}$  and  $E[\text{HR}]$  is the hydrogenated ligand energy, respectively.<sup>S5</sup>

On the other hand, we have investigated the formation energy (FE) per metal atom of  $\text{Au}_{25}(\text{SR})_{18}$  cluster for all thiol based aromatic ligand as described by Häkkinen et al.<sup>S6</sup> This can be calculated using equation as follows:

$$\text{FE} = E[\text{Au}_{25}(\text{SR})_{18}]^- + 18/2 * E[\text{H}_2] - 25 * E[\text{Au}_{\text{bulk}}] - 18 * E[\text{RSH}] / 25 \quad (2)$$

where,  $E[\text{Au}_{25}(\text{SR})_{18}]$  is the energy of the optimized cluster,  $E[\text{Au}_{\text{bulk}}]$  is the energy of Au atom within the FCC bulk gold,  $E[\text{H}_2]$  is the energy of isolated  $\text{H}_2$  molecule, and  $E[\text{RSH}]$  is the energy of RSH molecule calculated using DFT, considered SR as aromatic thiol ligand such as BT (benzenethiol), MBT (4-methylbenzenethiol), EBT (4-ethylbenzenethiol), IBT (4-isopropylbenzenethiol) and TBBT (4-tertbutylbenzenethiol), respectively.

All of the cohesive energy of the core (CE) and shell-to-core binding energy (CSBE) have been calculated using the thermodynamics stability model, as described by the Mpourmpakis and co-workers.<sup>S7</sup> The cohesive energies of the gold core and shell-to-core binding energies are calculated using the following equations:

$$E(\text{CE}) = \frac{E(\text{cluster}) - n * E(\text{Au}) - E(\text{shell})}{n + n(\text{shell-int})} \quad (3)$$

$$E(\text{CSBE}) = \frac{E(\text{cluster}) - E(\text{core}) - E(\text{shell})}{n(\text{shell-int})} \quad (4)$$

Where,  $E(\text{cluster})$  is the total energy of the cluster,  $E(\text{Au})$ s the energy of a single gold atom,  $E(\text{core})$  and  $E(\text{shell})$  are the single point energies of gold core and surrounding shell from the optimized geometries of the clusters,  $n$  and  $n(\text{shell-int})$  are the number of core gold atoms and the number of shell units interacting with the core.  $n(\text{shell-int})$  for  $[\text{Au}_{23}(\text{SR})_{16}]^-$ ,  $[\text{Au}_{25}(\text{SR})_{18}]^-$ ,  $[\text{Au}_{28}(\text{SR})_{20}]^0$  and  $[\text{Au}_{36}(\text{SR})_{24}]^0$  clusters are 8, 12, 14 and 16, respectively.

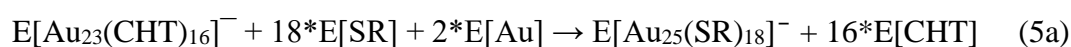
Here,  $E[\text{Au}_m(\text{SR})_n]$  is the total energy of the optimized  $\text{Au}_m(\text{SR})_n$  cluster and  $E[\text{Au}_m]$  and  $E[\text{SR}]$  are the single-point energies of the  $\text{Au}_m$  and thiol ligand (SR) from the optimized geometry of the cluster system.  $n$  is the number of SR unit in the geometry of the cluster.

Reaction energy (RE) is calculated by the difference between the sum of total energy of products and reactants using the following equation,

$$\text{RE} = \sum E(\text{product}) - \sum E(\text{reactant}) \quad (5)$$

Reaction energies (in eV) of the following conversion process are represented as follows:

Reaction -I,



Reaction -II,



Reaction -III,



Where, left and right hand side stand for the sum of total energies of the reactants  $[\text{Au}_m(\text{SR})_n]$  cluster; thiol ligands  $[\text{SR}]$  such as  $\text{SC}_6\text{H}_{11}$  (CHT= Cyclohexanethiol), BT, MBT, EBT, IBT, and TBBT; bulk gold (Au) atom; and the products respectively.

The average Au-SR binding energy or ligand interaction energy is calculated as a difference between the total energy of optimized cluster minus the energy of individual isolated structural configurations within the optimized cluster geometry.<sup>S8</sup> The average ligand interaction (LI) or Au-SR binding energy per SR unit is calculated using the following equation,

$$\text{LI} = E[\text{Au}_m(\text{SR})_n] - (E[\text{Au}_m] + n * E[\text{SR}])/n \quad (6)$$



## References:

- S1.** A. Das, T. Li, K. Nobusada, C. Zeng, N. L. Rosi, R. Jin, Nonsuperatomic  $[\text{Au}_{23}(\text{SC}_6\text{H}_{11})_{16}]^-$  Nanocluster Featuring Bipyramidal  $\text{Au}_{15}$  Kernel and Trimeric  $\text{Au}_3(\text{SR})_4$  Motif. *J. Am. Chem. Soc.*, 2013, **135** (49), 18264–18267.
- S2.** G. Kresse, J. Hafner, Ab initio molecular-dynamics simulation of the liquid-metal amorphous-semiconductor transition in germanium. *Phys. Rev. B*, 1993, **49**, 14251–14269.
- S3.** J. P. Perdew, J. A. Chevary, S. H. Vosko, K. A. Jackson, M. R. Pederson, D. J. Singh, C. Fiolhais, Atoms, Molecules, Solids, and Surfaces: Applications of the Generalized Gradient Approximation for Exchange and Correlation. *Phys. Rev. B*, 1992, **46**, 6671–6687.
- S4.** G. Kresse, D. Joubert, From ultrasoft pseudopotentials to the projector augmented-wave method. *Phys. Rev. B: Condens. Matter Mater. Phys.*, 1999, **59**, 1758.
- S5.** A. V. Nagarajan, R. J. Mosqueda, M. J. Cowan, R. Jin, D. R. Kauffman, G. R. Mpourmpakis, Mono-Palladium Substitution in Gold Nanoclusters Enhances  $\text{CO}_2$  Electroreduction Activity and Selectivity. *SN Applied Sciences.*, 2020, **2**, 680.
- S6.** S. Malola, H. Häkkinen, Electronic Structure and Bonding of Icosahedral Core–Shell Gold–Silver Nanoalloy Clusters  $\text{Au}_{144-x}\text{Ag}_x(\text{SR})_{60}$ . *J. Phys. Chem. Lett.*, 2011, **2**, 2316–2321.
- S7.** M. G. Taylor, G. Mpourmpakis, Thermodynamic stability of ligand-protected metal nanoclusters. *Nat. Commun.*, 2017, **8**, 15988.
- S8.** J. Jung, S. Kanga, Y-K. Han, Ligand effects on the stability of thiol-stabilized gold nanoclusters:  $\text{Au}_{25}(\text{SR})_{18}^-$ ,  $\text{Au}_{38}(\text{SR})_{24}$ , and  $\text{Au}_{102}(\text{SR})_{44}$ . *Nanoscale*, 2012, **4**, 4206–4210.
- S9.** L. Cheng, Y. Yuan, X. Zhang, J. Yang, Superatom Networks in Thiolate-Protected Gold Nanoparticles. *Angew. Chem. Int. Ed.*, 2013, **52**, 9035-9039.
- S10.** D. Jiang, S. H. Overbury, S. Dai, Structure of  $\text{Au}_{15}(\text{SR})_{13}$  and Its Implication for the Origin of the Nucleus in Thiolated Gold Nanoclusters. *J. Am. Chem. Soc.*, 2013, **135**, 8786–8789.

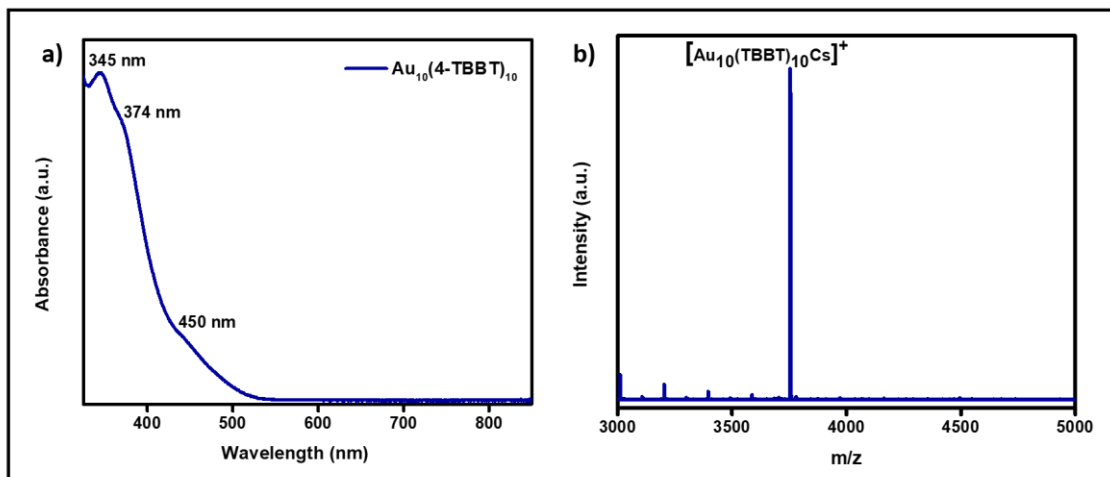


**Figure S1.** a) UV-visible spectrum and b) ESI-MS of  $\text{Au}_{10}(\text{TBBT})_{10}$ .

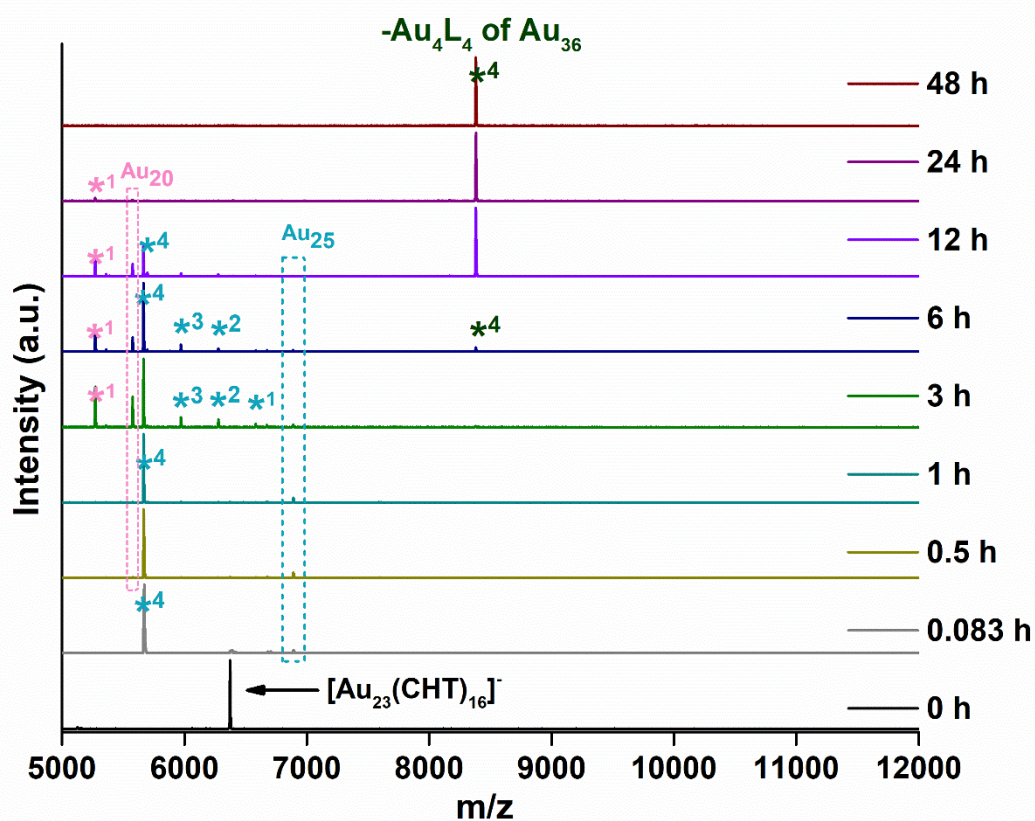


**Figure S2.** Time-dependent MALDI-MS spectra collected at different mass ranges showing the transformation process of  $[\text{Au}_{23}(\text{CHT})_{16}]^-$  nanocluster during the ligand exchange with BT ligand. Note: Dark green:  $\text{Au}_{36}$  nanocluster and its fragment, cyan:  $\text{Au}_{25}(\text{SR})_{18}$  and its fragment, pink:  $\text{Au}_{20}(\text{SR})_{15}$  nanocluster and its fragment, orange:  $\text{Au}_{15}$  nanocluster and its fragment. SR denotes BT ligand. (\*) Asterisk represent loss of AuL fragment where number with the asterisk represent how many AuL fragments are lost from the respective nanoclusters.

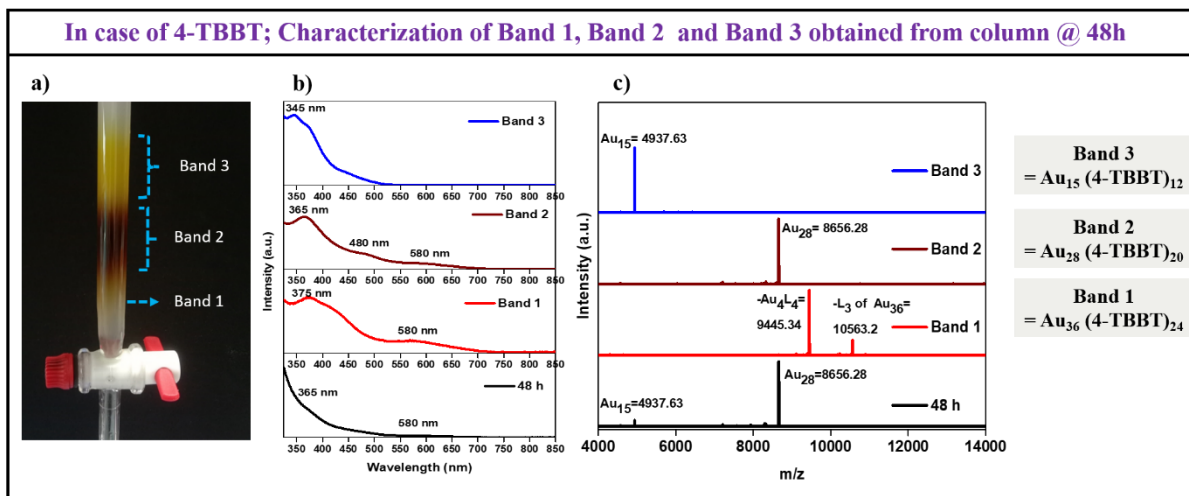


**Figure S3.** Characterization of bands obtained for 4-TBBT LER process after SEC. (a) Image of size exclusion chromatography showing separation of reaction mixture into three bands, (b) UV-visible absorption spectra of each band before and after separation, (c) MALDI-MS data of each band before and after separation.

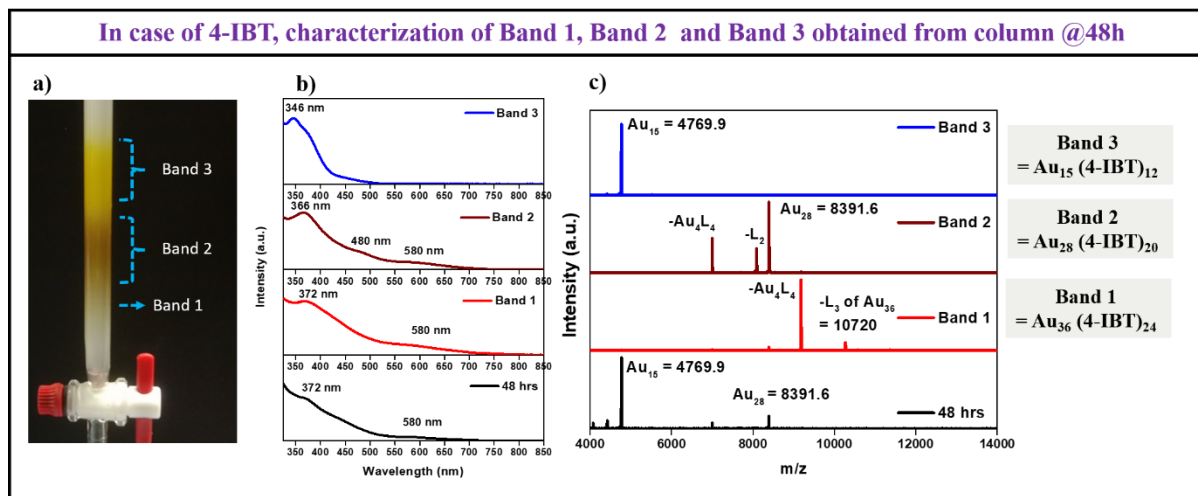


**Figure S4.** Characterization of bands obtained for 4-IBT LER process after SEC. (a) Image of size exclusion chromatography showing separation of reaction mixture into three bands, (b) UV-visible absorption spectra of each band before and after separation, (c) MALDI-MS data of each band before and after separation.

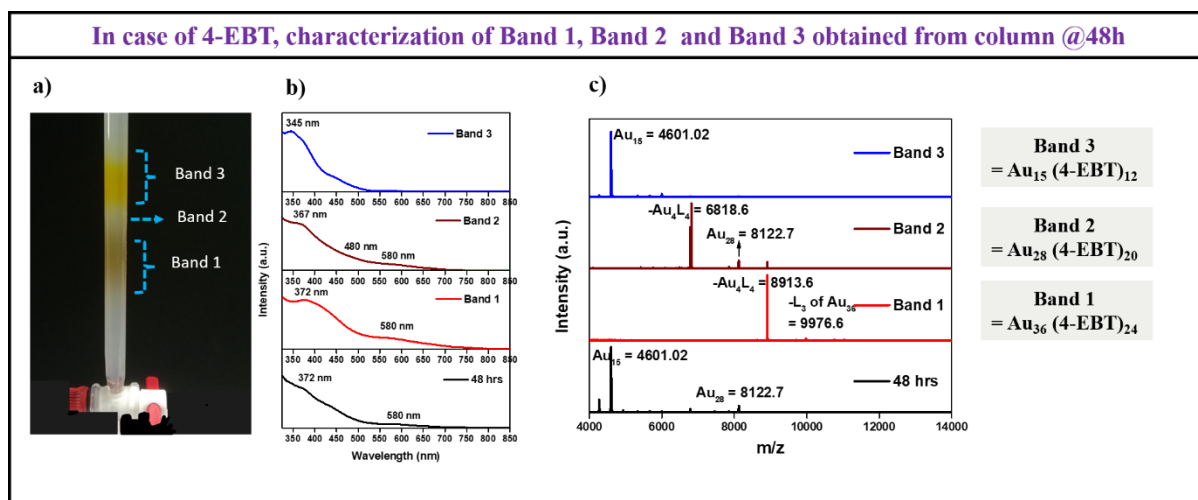


**Figure S5.** Characterization of bands obtained for 4-EBT LER process after SEC. (a) Image of size exclusion chromatography showing separation of reaction mixture into three bands, (b) UV-visible absorption spectra of each band before and after separation, (c) MALDI-MS data of each band before and after separation.

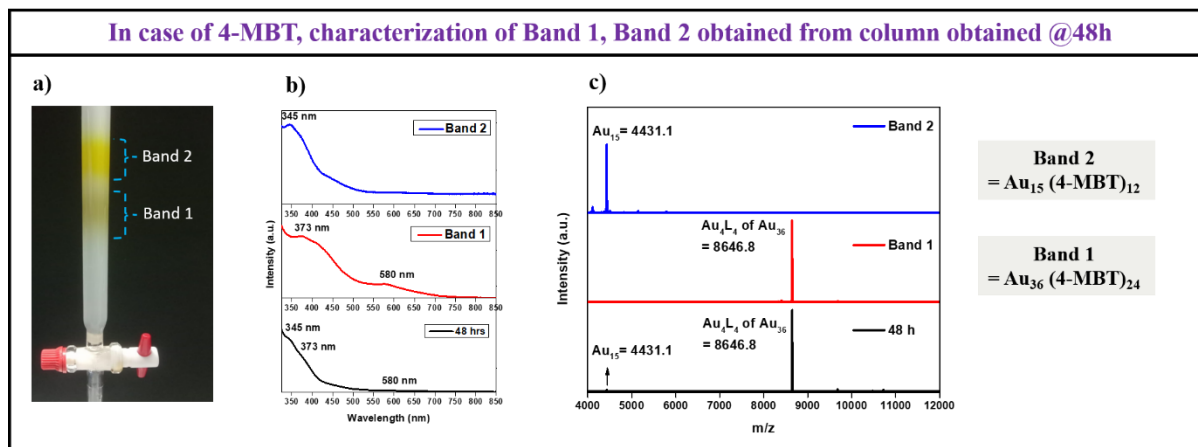


**Figure S6.** Characterization of bands obtained for 4-MBT LER process after SEC. (a) Image of size exclusion chromatography showing separation of reaction mixture into two bands, (b) UV-visible absorption spectra of each band before and after separation, (c) MALDI-MS data of each band before and after separation.

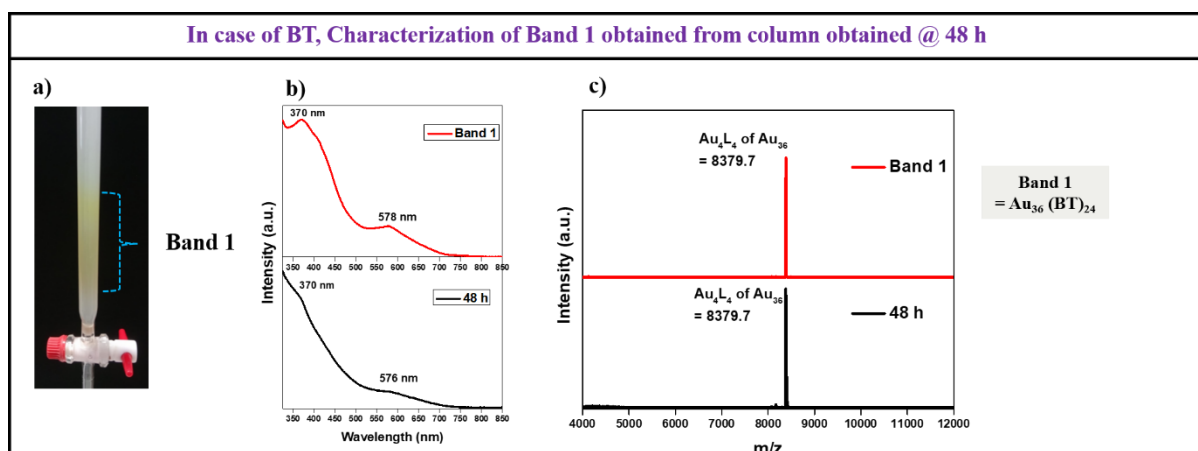


**Figure S7.** Characterization of bands obtained for BT LER process after SEC. (a) Image of size exclusion chromatography showing a single band (b) UV-visible absorption spectra of the band before and after separation, (c) MALDI-MS data of the band before and after separation.

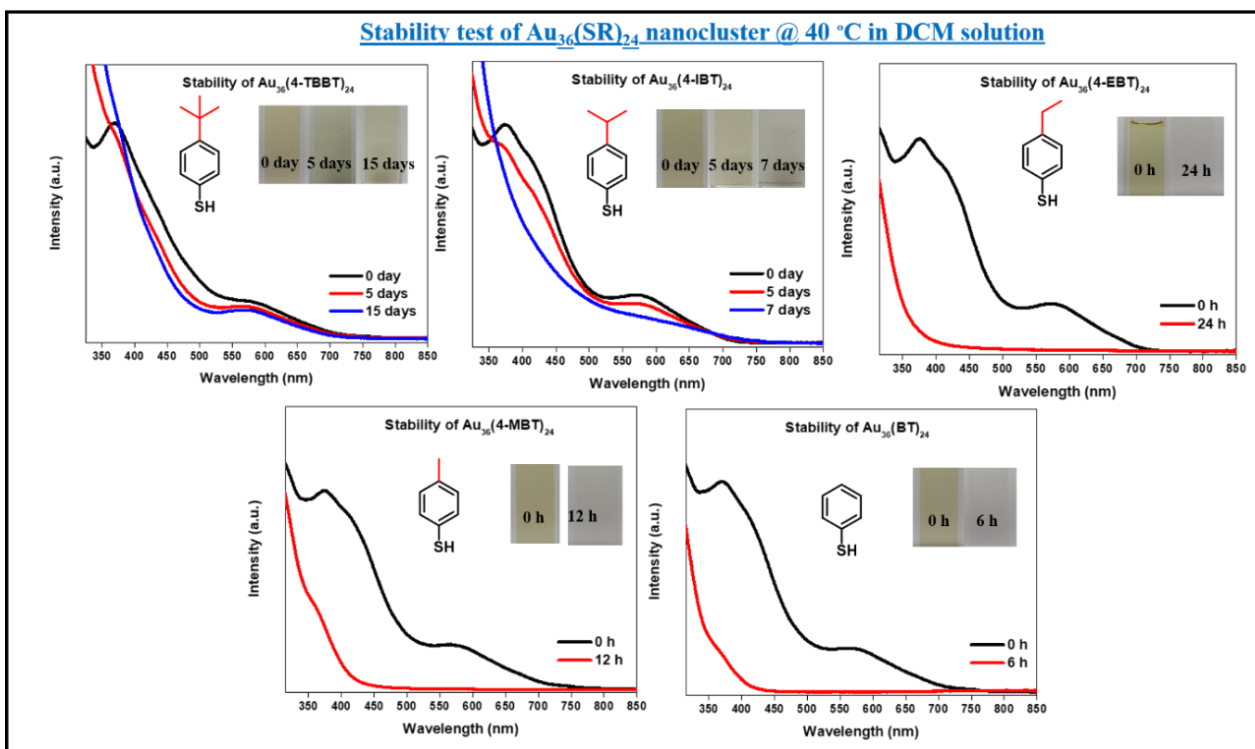


**Figure S8.** UV-visible spectra showing the stability test of  $\text{Au}_{36}(\text{SR})_{24}$ .

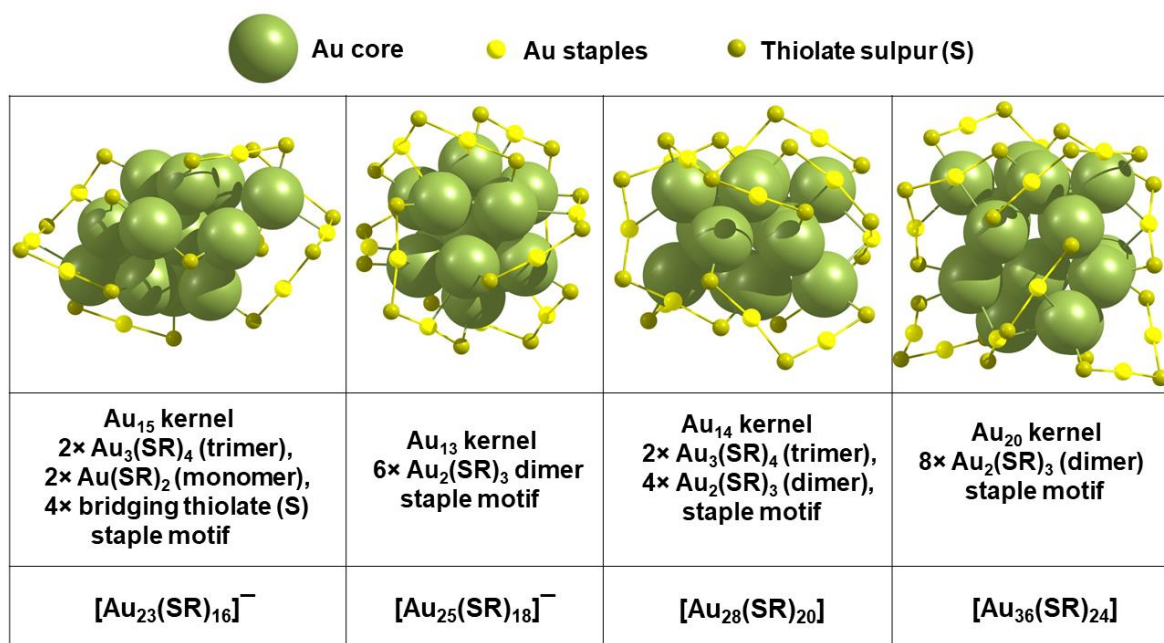


**Figure S9.** Different kernel structures with their respective type of staple motif within optimized geometries of Au<sub>n</sub>(SR)<sub>m</sub> clusters

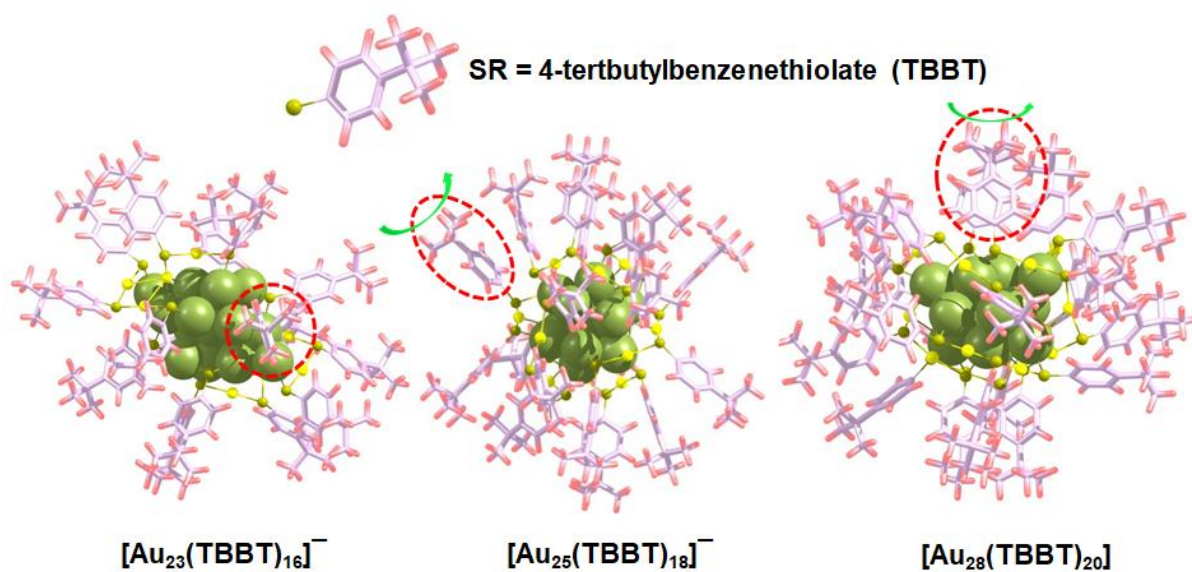


**Figure S10.** Optimized structure of  $[\text{Au}_{23}(\text{SR})_{16}]^-$ ,  $[\text{Au}_{25}(\text{SR})_{18}]^-$  and  $[\text{Au}_{28}(\text{SR})_{20}]$  clusters along with their respective staples with ligand (SR = TBBT). The red dashed circle indicates ligand rotating  $360^\circ$  against S-C (phenyl ring) bond along the green arrowed direction.

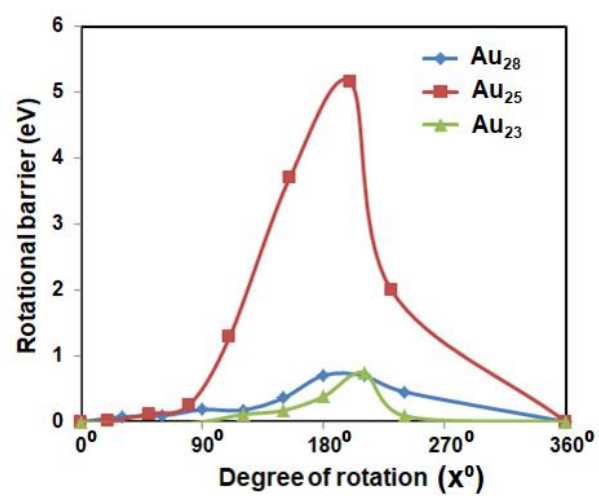


**Figure S11.** Rotational barrier for  $[\text{Au}_{23}(\text{TBBT})_{16}]^{-}$ ,  $[\text{Au}_{25}(\text{TBBT})_{18}]^{-}$ , and  $\text{Au}_{28}(\text{TBBT})_{20}$  clusters

**Table S1.** Calculated values of average ligand removal reaction energy (LRE) and rotational barrier for  $\text{Au}_n(\text{TBBT})_m$  clusters.

System	LRE ( eV )	Barrier (eV)
$\text{Au}_{23}(\text{TBBT})_{16}$	-3.59	0.75
$\text{Au}_{25}(\text{TBBT})_{18}$	-3.84	5.15
$\text{Au}_{28}(\text{TBBT})_{20}$	-3.55	0.70

**Table S2.** Formation energy (FE) values for all thiol ligands in  $[\text{Au}_{25}(\text{SR})_{18}]^-$  clusters.

System	Thiol ligands (SR)	FE (eV)
$[\text{Au}_{25}(\text{SR})_{18}]^-$	BT	0.08
	MBT	0.09
	EBT	0.09
	IBT	0.12
	TBBT	0.16

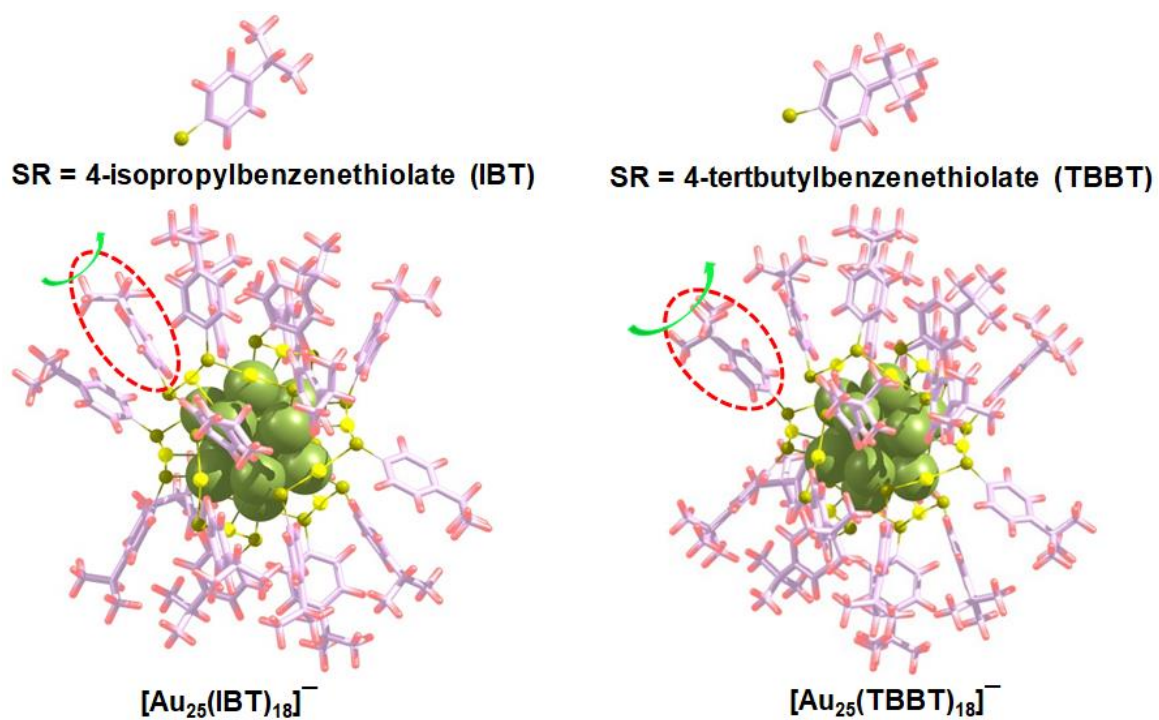


**Figure S12.** Optimized structure of  $[\text{Au}_{25}(\text{IBT})_{18}]^{-}$  and  $[\text{Au}_{25}(\text{TBBT})_{18}]^{-}$  clusters along with their respective staples with ligands (SR = 4-IBT, 4-TBBT). The red dashed circle indicates ligand rotating  $360^\circ$  against S-C (phenyl ring) bond along the green arrowed direction.

**Table S3.** Rotational barrier values for thiol based IBT and TBBT ligand in  $[\text{Au}_{25}(\text{SR})_{18}]^-$  clusters.

System	Barrier (eV)
$\text{Au}_{25}(\text{IBT})_{18}$	2.40
$\text{Au}_{25}(\text{TBBT})_{18}$	5.15

**Table S4.** Core cohesive energy (CE) and shell to core binding energy (CSBE) of all  $\text{Au}_m(\text{SR})_n$  clusters.

System	$[\text{Au}_{23}(\text{SR})_{16}]^-$		$[\text{Au}_{25}(\text{SR})_{18}]^-$		$\text{Au}_{28}(\text{SR})_{20}$		$\text{Au}_{36}(\text{SR})_{24}$	
	CE	CSBE	CE	CSBE	CE	CSBE	CE	CSBE
CHT	-2.47	-3.27	--	--	--	--	--	--
BT	-2.37	-3.06	-1.83	-1.63	-1.71	-1.36	-1.90	-1.51
MBT	-2.35	-3.00	-1.82	-1.61	-1.70	-1.32	-1.90	-1.50
IBT	-2.32	-2.94	-1.81	-1.59	-1.69	-1.33	-1.88	-1.50
TBBT	-2.32	-2.93	-1.81	-1.59	-1.71	-1.35	-1.88	-1.50

**Table S5.** Reaction energy (RE) values (eV) for all the conversion process given in Text S1 via ligand (SR= BT, MBT, EBT, IBT, TBBT) exchange.

<b>Ligand</b>	<b>Reaction-I</b>	<b>Reaction-II</b>	<b>Reaction-III</b>
<b>BT</b>	-1.35	-5.34	-6.01
<b>MBT</b>	-0.06	-4.83	-5.91
<b>EBT</b>	-0.16	-5.77	-5.72
<b>IBT</b>	0.50	-5.49	-5.73
<b>TBBT</b>	0.33	-5.98	-5.77

**Table S6.** Average ligand interaction energy (eV/SR) of all the Au<sub>m</sub>(SR)<sub>n</sub> clusters.

	<b>System</b>	<b>[Au<sub>23</sub>(SR)<sub>16</sub>]<sup>-</sup></b>	<b>[Au<sub>25</sub>(SR)<sub>18</sub>]<sup>-</sup></b>	<b>Au<sub>28</sub>(SR)<sub>20</sub></b>	<b>Au<sub>36</sub>(SR)<sub>24</sub></b>
<b>Thiol ligands (SR)</b>	<b>CHT</b>	-2.89	--	--	--
	<b>BT</b>	-2.81	-2.84	-3.08	-2.99
	<b>MBT</b>	-2.72	-2.77	-3.03	-2.93
	<b>IBT</b>	-2.64	-2.74	-3.01	-2.90
	<b>TBBT</b>	-2.65	-2.75	-3.02	-2.89

**Table S7.** Core cohesive energy (CE), shell to core binding energy (CSBE), average ligand interaction energy (LI) values of intermediate  $[\text{Au}_{25}(\text{SR})_{18}]^-$  clusters and reaction energy (RE) values for Reaction-III among thiol ligands (SR = BT, MBT, EBT, IBT, TBBT) considered.

<b>Ligand</b>	<b>CE</b>	<b>CSBE</b>	<b>LI</b>	<b>RE</b>
<b>BT</b>	-1.83	-1.63	-2.84	-6.01
<b>MBT</b>	-1.82	-1.61	-2.77	-5.91
<b>EBT</b>	-1.82	-1.61	-2.77	-5.72
<b>IBT</b>	-1.81	-1.59	-2.74	-5.73
<b>TBBT</b>	-1.81	-1.59	-2.75	-5.77

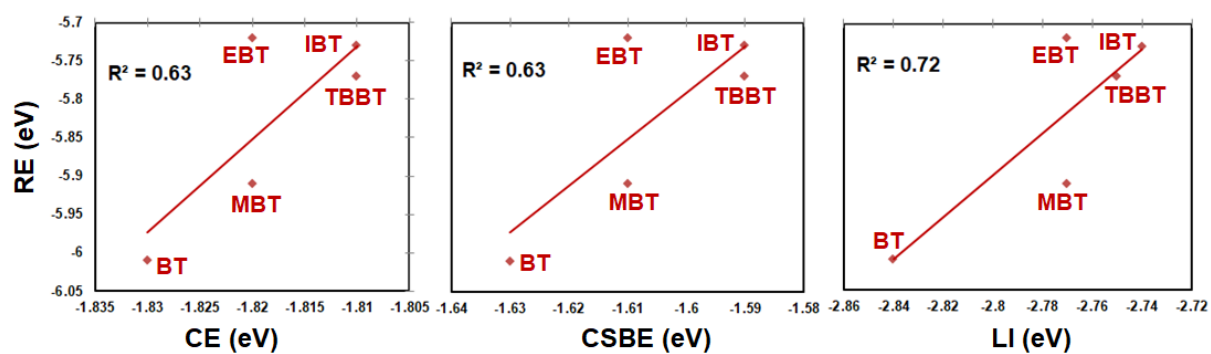


**Figure S13.** Reaction energy (RE) following Reaction-III plotted against (a) core cohesive energy (CE), (b) shell to core binding energy (CSBE) and (c) average ligand interaction (LI) of  $[\text{Au}_{25}(\text{SR})_{18}]^-$  clusters, where SR = BT, MBT, EBT, IBT, TBBT.

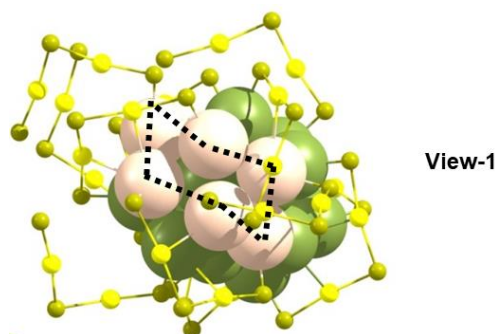


**Figure S14.** Alternative view of a proposed cluster of Au<sub>26</sub> core along with dissociating cyclic chair conformation of Au<sub>6</sub> unit composed of two Au<sub>3</sub> units.

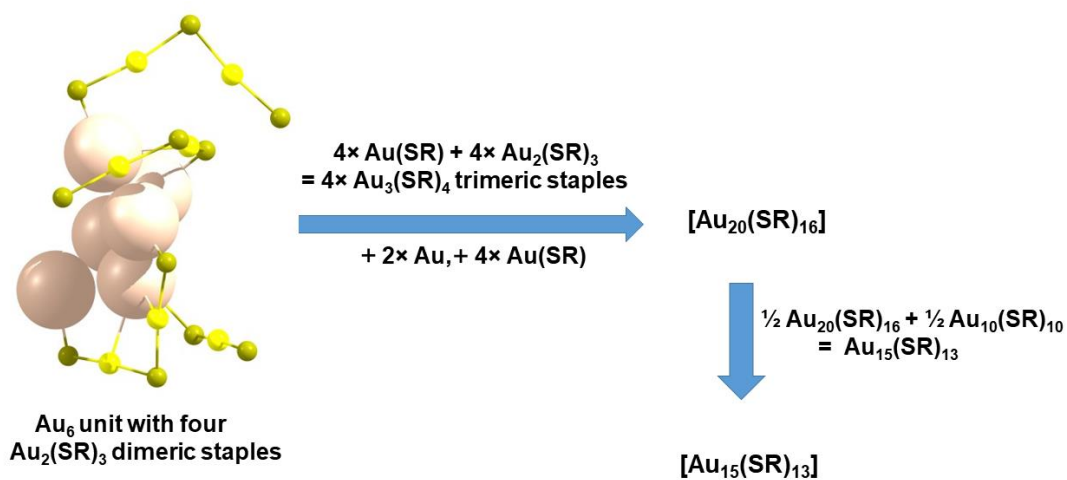


**Figure S15.** A proposed mechanistic transformation of dissociating  $\text{Au}_6$  unit with four dimeric staples to  $\text{Au}_{20}(\text{SR})_{16}$  and  $\text{Au}_{15}(\text{SR})_{13}$  clusters during the process.<sup>S8,S9</sup> The pink, yellow and green colors represent  $\text{Au}_6$  unit, staple Au and sulphur atoms, respectively. The ligands are omitted for visual convenience. Though, we have not done any further investigation with these clusters as well.

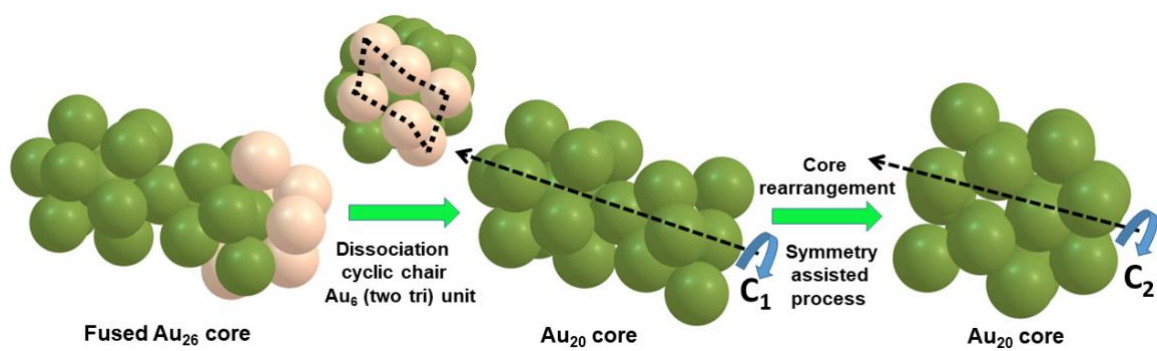


**Figure S16.** A proposed mechanism for dissociation of Au<sub>6</sub> unit and symmetry assisted complex rearrangement of Au<sub>20</sub> core isomerization.